Design Aspects for Wide-Area Monitoring and Control Systems

MAREK ZIMA, STUDENT MEMBER, IEEE, MATS LARSSON, MEMBER, IEEE, PETR KORBA, CHRISTIAN REHTANZ, SENIOR MEMBER, IEEE, AND GÖRAN ANDERSSON, FELLOW, IEEE

Invited Paper

This paper discusses the basic design and special applications of wide-area monitoring and control systems, which complement classical protection systems and Supervisory Control and Data Acquisition/Energy Management System applications. Systemwide installed phasor measurement units send their measured data to a central computer, where snapshots of the dynamic system behavior are made available online. This new quality of system information opens up a wide range of new applications to assess and actively maintain system's stability in case of voltage, angle or frequency instability, thermal overload, and oscillations. Recent developed algorithms and their design for these application areas are introduced. With practical examples, the benefits in terms of system security are shown.

Keywords*—Power system control, power system dynamic stability, power system monitoring, power system protection, predictive control, system protection scheme.*

I. INTRODUCTION

Power supply has become so important for the entire society that large efforts must be made to prevent power systems from collapse scenarios. Recent collapse events all over the world show the urgent need for stabilizing power systems beyond the common technologies. Increasing demands on the power system will increase further the likelihood of system problems such as instabilities and collapses. One promising way is to provide a systemwide protection and control complementary to the conventional local equipment and the Supervisory Control and Data Acquisition/Energy Management System (SCADA/EMS) system.

While it is not possible to predict or prevent all contingencies that may lead to power system collapse, a wide-area monitoring and control system that provides a reliable security prediction and optimized coordinated actions is able to mitigate or prevent large area disturbances. The main tasks are early recognition of instabilities, increased power system availability, operation closer to the limit, increased power transmission capability with no reduction in security, better access to low-cost generation, fewer load shedding events, and minimization of the amount of load shedding.

The main disadvantages of common systems consist in the inappropriate steady-state system's view like in today's SCADA/EMS system, or in uncoordinated local actions like in decentralized protection devices. The solution for this is a departure from the SCADA-based approach to a dynamic measurement system using synchronized phasor measurement units (PMUs). Together with the stability assessment and stabilization algorithms, such a system is called a wide-area monitoring and control (WAMC) system in the following. PMUs offer the measurement of phasors of voltage and currents together with a satellite triggered time stamp in time intervals down to 20 ms. Single installations of such units are in an experimental stage in many power systems. This paper concentrates besides the introduction of the new wide-area monitoring and control system setup on the stability assessment of various kinds of phenomena. The proposed algorithms are designed especially for the opportunities that are offered by the dynamic system's view.

The paper is organized as follows. First, the platform and software architecture of WAMC is presented. After that some algorithms for power system applications are presented: frequency stability assessment, oscillation detection assessment, and voltage stability assessment. The proposed scheme is finally demonstrated in an example using a realistic power system.

Manuscript received April 30, 2002; revised December 1, 2003.

M. Zima is with the EEH—Power Systems Laboratory, ETH Zürich, Zürich CH-8092, Switzerland, and also with ABB Switzerland Ltd., Baden CH-5401, Switzerland (e-mail: zima@ch.abb.com).

G. Andersson is with the EEH—Power Systems Laboratory, ETH Zürich, Zürich CH-8092, Switzerland (e-mail: andersson@eeh.ee.ethz.ch).

M. Larsson P. Korba is with Corporate Research, ABB Switzerland Ltd., Baden-Dättwil CH-5405, Switzerland (e-mail: mats.larsson@ch.abb.com; petr.korba@ch.abb.com).

C. Rehtanz is with the ABB (China) Ltd., Beijing 100016, China; (e-mail: christian.rehtanz@ieee.org).

Digital Object Identifier 10.1109/JPROC.2005.846336

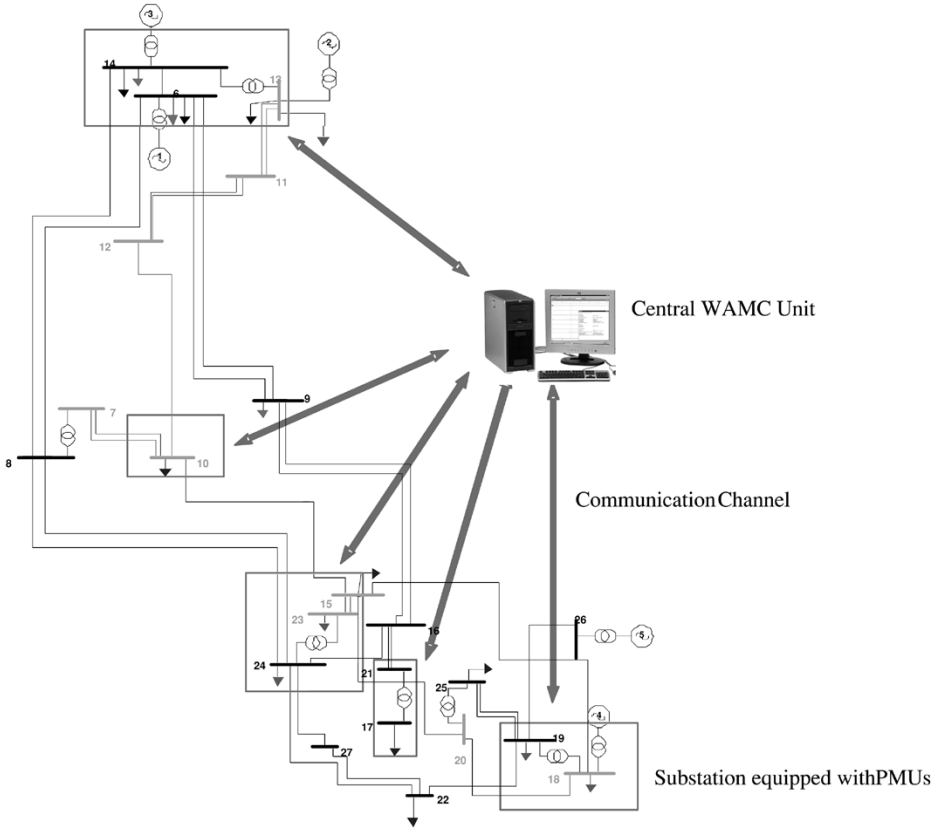

Fig. 1. Proposed WAMC configuration for a real power system.

II. Proposed Platform for WAMC

The core idea of the WAMC systems is the centralized processing of the data collected from various locations of a power system, aiming at the evaluation of the actual power system operation conditions with respect to its stability limits. Although the particular application range of WAMC is quite wide, depending on the addressed phenomena, the fundamental structure remains the same. In this section, we discuss this fundamental structure of the proposed WAMC system both from the hardware and software point of view. The hardware can be explained based on the three stages of the data handling in WAMC, as shown in Figs. 1 and 2:

- data acquisition;
- data delivery;
- data processing.

Power systems are today operated closer to their stability limits than at any time before, which makes them very sensitive to disturbances, and the monitoring and control issues have shifted from the preventive to the emergency ones. The dynamics and nonlinearities play a significant role in the critical power system operation. To properly observe the system dynamics, the needed measurements should possess the following characteristics: they must be taken from different network locations, with high sampling rate and at the same time instant. The latter one requires a high degree of synchronization of the measurement instant. This problem is faced also in the case of the line differential relays, where it is solved by the mutual communication of the two relays placed at both ends of the line. However, when the synchronization of many devices placed in very geographically distant locations is necessary, the only feasible way is utilization of the global positioning system (GPS) time synchronization signal. This concept is employed in the measurement devices called PMUs. In the PMU case, there is no need for communication between the units. Therefore, we see PMUs as the ideal candidate for the centralized structure of WAMC, especially when considering the capability of PMUs to provide the various types of data and preprocess them. The quantities to be measured by PMUs and the locations for the installation of the PMUs are dependent on many factors. The most significant criteria are the instability phenomena, which should be mitigated, followed by the practical economic aspects such as utilization of the existing communication infrastructures, etc. Transmission of the measured data (alternatively, also transmission of the control command in the opposite direction) is arranged by means of the communication channels. They have to be dedicated to this purpose in the case of the control functionality of WAMC in order to guarantee the command execution specified times. If this is not possible, the use of the available TCP/IP network in the substations is recommended. The data are then collected in the central computer equipped with the appropriate software. The software structure is modular, as shown in Fig. 3. The software packages can be divided into two groups.

- Instability assessment and control applications; they will be discussed in the next section.

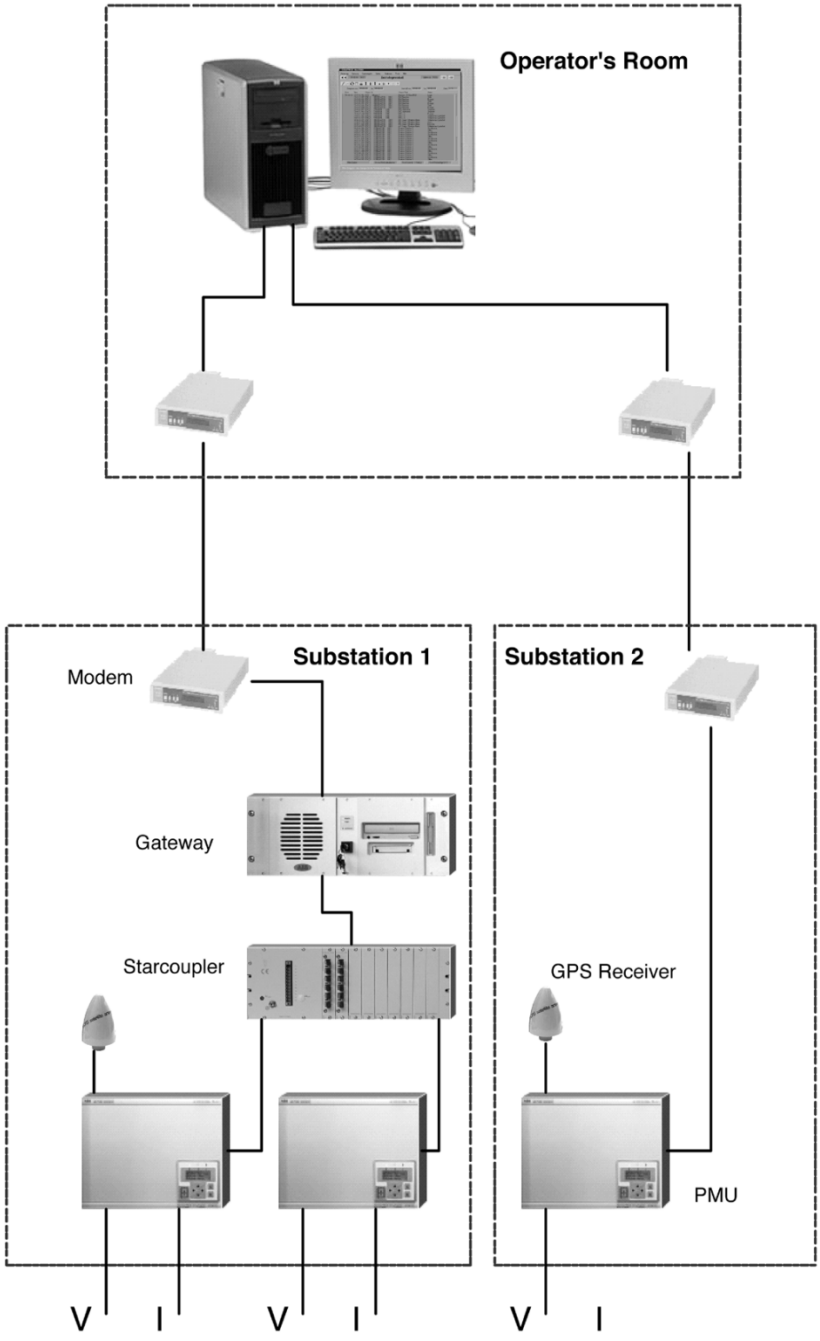

Fig. 2. Example of the hardware architecture of the proposed WAMC system.

- Auxiliary programs common to all installations of WAMC:
  1) Object linking and embedding (OLE) for a process control (OPC) server connecting the PMUs to the platform.
  2) The platform itself—storing the data and linking the software packages together.
  3) A GUI interpreting the result of the measurement and instability assessment to the user (dispatcher/operator); history data package.
  4) OPC history data access (OPC HDA) provides a set of standard interfaces that allow clients to access historical archives of measurements to retrieve and store the data in a uniform manner.

III. Overview of Developed Algorithms

The position of the instability assessment and control algorithms within the software architecture of the proposed WAMC system are shown in Fig. 3. The nature of instability phenomena and the power system topology properties have an impact on the further categorization of the WAMC algorithms from the software packages point of view:

- algorithms requiring a full observability of the network—*Frequency Instability Assessment, Voltage Instability Assessment of Meshed Networks*.
- algorithms not requiring an entire network observation—*Oscillation Detection Assessment, Voltage*

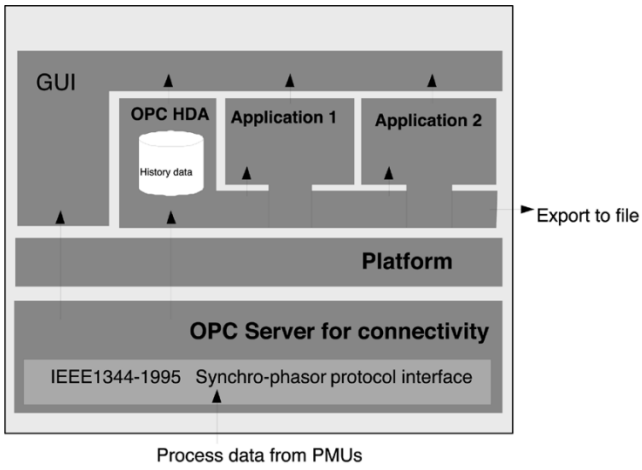

Fig. 3. Software architecture of the proposed WAMC. Black arrows represent the data flow.

Instability Assessment Of the Transmission Corridors, Line Temperature Monitoring.

Wide-area control of flexible ac transmission systems (FACTS) can be applied based on all of these assessment algorithms. The first group of the algorithms needs, as prerequisite, almost the complete network observation, which can be expressed in terms of the following data availability/knowledge: network topology, all voltage magnitudes and angles, all branch currents magnitudes and angles and selected loads, and generator currents' magnitudes and angles. This is achieved by the application of the multistage linear state estimation using the measured PMU data. The basic principle is described in [1] and [2]. The other algorithms are explained in the following subsections.

A. Frequency Instability Assessment [3]

Frequency stability is a major concern in the operation of power systems. Following severe disturbances, such as the outage of a large generation station or an interconnection to a neighboring system, the average frequency will change in the system. Unless the frequency drop is arrested before the frequency reaches 47–48 Hz in a 50 Hz system (or 57–58 Hz in a 60-Hz system), thermal units are tripped to avoid damage from prolonged underfrequency operation and this worsen the situation even further. In these situations, it may therefore be necessary to disconnect loads to preserve system integrity. Underfrequency load shedding (UFLS) [4] is the most widely used protection against frequency instability. Typically, load is shed based on a local frequency measurement in several steps of 5%–20% each. Typical threshold values are 57–58.5 Hz for 60-Hz systems or 48–48.5 Hz for a 50-Hz system. Usually, there is also a time delay intended for noise rejection. The drawbacks of these types of relays is their slow response, which is due to the fact that they wait until the frequency is already low before ordering load shedding and that overshedding is commonly ordered by these relays. It is well known that the power mismatch following the outage of a generator or a tie line can be calculated from the initial rate of change of the frequency and the system inertia constant according to the formula [5]

$$\Delta P = 2H_{\text{system}}\frac{d\omega}{dt}. \tag{1}$$

This value can be used as an indication of the amount of load that has to be shed to arrest further frequency decline. Several papers have proposed UFLS relays based on this measurement. For example, [6]–[9] have presented so-called adaptive UFLS using only local measurements. It avoids the slow response associated with the conventional approach. However, since it lacks coordination, it is difficult to tune them in such a way that overshedding is avoided. A further drawback of both types of relays is that their tuning depends on offline assumptions of the loads' response to frequency deviations and the remaining system inertia. Since these vary from disturbance to disturbance, the relays must be tuned for the worst case scenario and thus they may take excessive control actions, possibly resulting in overfrequency.

The proposed approach is based on a predictive method for frequency stability and wide-area phasor measurements and avoids the drawbacks of conventional relays. The control actions are based on online measurements instead of on conservative offline assumptions. A single-machine equivalent model [5] is formed online and used for the monitoring and control of the frequency and for calculating the amount of necessary load or generation shedding to maintain the required frequency within given bounds. This method is applicable also for generation-rich islands, where over-frequency might be a problem—the control actions reduce the generation instead of load. Examples of control actions may be generation tripping or fast valving. The frequency dynamics are determined by the differential equation

$$\frac{d\omega_{\text{avg}}}{dt} = \frac{1}{2H_{\text{system}}}(P_m - P_e) \tag{2}$$

where H_i is the inertia constant of generator i and H_{system} is the system inertia constant defined as follows:

$$H_{\text{system}} = \sum_{1\ldots N} H_i \tag{3}$$

$$P_m = \sum_{1\ldots N} P_{m,i} \tag{4}$$

$$P_e = P_{\text{loss}} + \sum_{1\ldots M} P_{l,i} \tag{5}$$

for an island with N generators, M load buses, and active power losses P_{loss}. P_m is the total mechanical power delivered to the generator shafts by the turbines and P_e is the total electrical load on the generators. Based on (2)–(5), a single-machine equivalent model can be constructed

$$\frac{d\Delta x}{dt} = A_{\text{ode}}\Delta x + B_{\text{ode}}\Delta k + E_{\text{ode}}\Delta d \tag{6}$$

$$\Delta y = C_{\text{ode}}\Delta x \tag{7}$$

where x is the dynamic state containing the average frequency, Δk is an external input modeling load shedding and Δd a disturbance input modeling e.g., generator tripping.

Matrices $A_{\text{ode}}, B_{\text{ode}}, C_{\text{ode}}$, and E_{ode} contain corresponding sensitivity coefficients. The current power mismatch in the system can be calculated as

$$\Delta d = 2H_{\text{system}} \frac{d\omega_{\text{avg}}}{dt}. \tag{8}$$

This power mismatch will change due to load frequency and voltage sensitivity as well as applied control actions. The quantity $(d\omega_{\text{avg}})/(dt)$ is a measured signal and H_{system} a parameter to be supplied by the wide-area measurement system. The calculated power mismatch thus corresponds to the amount of generation or load lost only at the instant of disconnection, i.e., measurement point 1. Using the power mismatch, the predicted steady-state average frequency can be calculated as

$$\Delta y^* = -C_{\text{ode}} A_{\text{ode}}^{-1} (B_{\text{ode}} \Delta k + E_{\text{ode}} \Delta d). \tag{9}$$

At this stage, it is assumed that no load shedding control is made, i.e., $\Delta k = 0$, so the predicted steady-state output is written

$$\Delta y^* = -C_{\text{ode}} A_{\text{ode}}^{-1} E_{\text{ode}} \Delta d \tag{10}$$

Subsequently, the predicted steady state frequency is found using

$$y^* = \Delta y^* + y_0. \tag{11}$$

This value of the steady-state frequency is used as the frequency stability indicator—if the steady-state frequency is unacceptable, corrective controls such as load shedding must be applied. For more details, see [3].

B. Oscillation Stability Assessment

Electromechanical oscillations occur in power systems due to lack of damping torque at the generator rotors. Oscillations of the generators rotors cause oscillations of other power system variables, e.g., bus voltage and frequency, and reactive and active powers on transmission lines. Depending on the number of involved generators and the size of the power network, power system oscillations have been reported in the range of 0.05–2 Hz [10]. Local oscillations lie in the upper part of the above range and consist of oscillations of a single generator or a group of generators against the rest of the system. Interarea oscillations lie in the lower part of the range and comprise the oscillations between groups of generators. In general, power system oscillations are ever-present, poorly damped, and not dangerous as long as they do not become unstable. The objective has been to develop an algorithm for a real-time monitoring of oscillations from online measured signals; in other words, to estimate the parameters characterizing the electromechanical oscillations such as frequency and damping and to present this information to the operator in a user-friendly environment of the operator station. This kind of information can hardly be obtained only by watching the measured signals displayed in the time domain. Here, a model-based estimation method has been employed. It

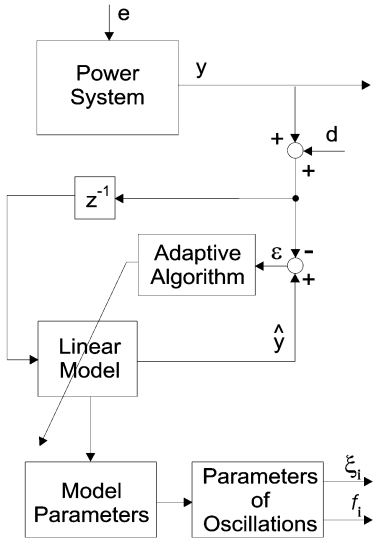

Fig. 4. Basic scheme for the proposed detection of power system oscillations.

utilizes an autoregressive (AR) model (12) which can also be rewritten as (13) where $\varepsilon = \hat{y}(k \,|\, k-1) - y(k)$

$$\hat{y}(k \,|\, k-1) = \sum_{i=1}^{n} a_i(k) y(k-i) \tag{12}$$

$$y(k) = \sum_{i=1}^{n} a_i(k) y(k-i) - \varepsilon(k). \tag{13}$$

Fig. 4 shows the proposed approach to the model-based detection of oscillations. The power system is excited by a sequence of disturbances represented by the noise e and modeled by the AR model with adjustable (time-varying) coefficients. The appropriate signal (a measurement provided by a PMU) is selected either based on results of modal analysis of the power system model or consulting an experienced operator in order to ensure a possibly high observability of the modes of interest [11]. The measured signal y may contain some measurement noise d. An adaptive algorithm recursively optimizes the criterion (14) and yields the optimal parameters of the AR model, generating possibly the same sequence of data $\hat{y}$ as the measured y. The goal is to obtain the parameters of oscillations characterized by their frequency f_i and damping ξ_i. They are obtained repeatedly (once per given period, so-called refresh time T_r) from the AR model for the set of its n parameters $a_i(k)$. Therefore, the first step of the presented approach is to estimate recursively these coefficients $a_i(k)$ that minimize the sum of squared prediction errors (14)

$$J = \min_{a_i(k)} \sum \varepsilon^T \varepsilon = \min_{a_i(k)} \sum (\hat{y}(k \,|\, k-1) - y(k))^2 \tag{14}$$

where $\hat{y}(k \,|\, k-1)$ denotes the predicted value of $y(k)$ based on the measurements available only up to time $k-1$. Recall that the poles of this model contain the required information about the time-varying system dynamics, which depends on the operating point of the power system. The poles can be

calculated solving the characteristic equation (15) for a set of actual values of $a_i(k)$ frozen at time k.

$$z^n - a_1(k)z^{n-1} - \cdots - a_{n-1}(k)z - a_n(k) = 0. \quad (15)$$

The assumption here is that the power system is operated at the same operating point for a certain period that enables the estimated coefficients to converge. Indeed, this is no constraint in practice, since the estimated model parameters converge to their new values fast enough compared to the dynamics of the power system, if e.g., the algorithm proposed here is employed

$$z = \frac{1 + sT_s/2}{1 - sT_s/2}. \quad (16)$$

The estimated dynamic model is to be converted from the discrete-time domain into the more convenient continuous one using some well-known integrator approximation and the known sampling period T_s. In order to get the estimates of the relative damping in percentages and the frequency in hertz, the most suitable conversion seems to be based on Tustin's approximation (16). This one has the property of mapping the left half s-plane exactly into the unit disk in z-plane and *vice versa*. Hence, its advantage is that the stable discrete-time domain is transferred into the stable continuous-time domain

$$s_i = \alpha_i + i\omega_i. \quad (17)$$

The relationship between the discrete-time operator z and the continuous-time operator s to obtain the required continuous-time poles is for the bilinear Tustin's approximation given by (16). The complex poles (17) calculated from the continuous-time model characterize the oscillations

$$w_i = 2\pi f_i. \quad (18)$$

Its real part α_i gives the information about the absolute damping and the imaginary part ω_i about the natural frequency, and f_i from (18) is the sought oscillatory frequency in hertz.

$$\xi_i = -100\frac{\alpha_i}{\sqrt{\alpha_i^2 + \omega_i^2}}. \quad (19)$$

A practical measure for the assessment of the damping of oscillations is not the absolute damping α_i but rather the relative damping introduced in (19) yielding the normalized values in percent. A working power system is stable. This means in terms of the relative damping that $0 < \xi_i < 100, \forall i$. Note that the optimal model parameters $a_i(k)$ must be updated recursively once per sampling period T_s for each new measurement $y(k)$. However, the solution of the characteristic equation, which yields the required information about the frequency and the damping, can be calculated only once per refresh time T_r, where $T_r \gg T_s$ in order to economize the computational power. It has turned out in our tests with measured data that among all considered approaches (recursive least squares, least mean squares, and Prony's methods [12]–[14]), the adaptive Kalman filtering technique [15] is the most suitable tool to identify the optimal model parameters. This approach has shown the smallest prediction error and the shortest estimation time, i.e., the number of iterations necessary for the parameters to converge. At the same time, applying this method to different measured signals, the results were not very sensitive with regard to the set of the tuning parameters. The standard set of recursive equations to be solved online is for the Kalman Filter known to be (20); see, e.g., [15]

Table 1
Variables of Algorithm for Parameter Identification

Variable	Description
k	discrete time (actual iteration)
n	number of the estimated parameters
$y(k)$	actual measurement; desired model response at time step k
$u(k)$	buffered past n measurements, $u(k) = [y(k-1), \ldots, y(k-n)]$
$\varepsilon(k)$	actual prediction error at time step k
$p(k)$	vector of estimated model parameters, $a_i(k) = [1, -p_1(k), \ldots, -p_n(k)]$
$K(k)$	correlation matrix of the estimation error
$g(k)$	calculated Kalman-gain at time step k
Q_m	correlation of the measurement noise
Q_p	correlation matrix of the process noise

$$\begin{aligned} g(k) &= \frac{K(k-1)u(k)}{u^T(k)K(k-1)u(k) + Q_m} \\ \varepsilon(k) &= u^T(k)p(k-1) - y(k) \\ p(k) &= p(k-1) + \varepsilon(k)g(k) \\ K(k) &= K(k-1) - g(k)u^T(k)K(k-1) + Q_p. \end{aligned} \quad (20)$$

The meaning of the parameters and variables of (20) are described in Table 1.

To ensure good numerical robustness of the standard estimation algorithm, (20) has been extended by some additional equations [see (21)]. The covariance matrix $K(k)$ is enforced here to remain symmetrical, and for a better parameter tracking, a regularized constant trace algorithm is used with $c_1/c_2 \cong 10^4$

$$\begin{aligned} K(k) &= \frac{K(k) + K^T(k)}{2} \\ K(k) &= \frac{c_1 K(k)}{\mathrm{tr}(K(k))} + c_2 Q_p. \end{aligned} \quad (21)$$

Note that all the variables can be initialized with zeros, except for the covariance matrix $K(0)$, which should be initialized with a unity matrix multiplied by a big constant. The most important parameter for tuning is the model order n. Its selection is one of the most important aspects of the use of AR models. If one selects a model with too low order, the obtained spectrum will be highly smoothed. On the other hand, if the order is too high, faked low-level peaks in the spectrum will be introduced. Note that dominant oscillations correspond to the lowest peak in the spectrum; see Fig. 13. An effective and systematic method to find out the appropriate model order n is to combine the criteria proposed by Akaike (see, e.g., [16]) followed by a trial-and-error procedure. The measured signal $y(k)$ is filtered through a digital bandpass filter (with the cutoff frequencies 0.1 and 2 Hz mentioned earlier). If the bandpass filtered signal consists for a short period rather of only noise (low signal power) than of realistic data,

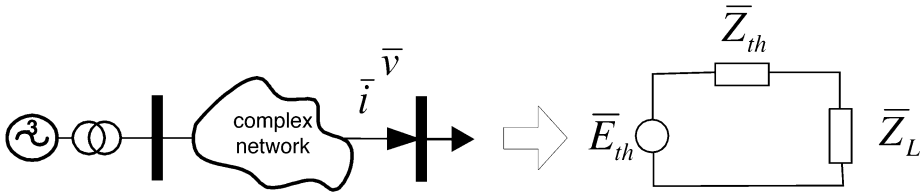

Fig. 5. Estimation of the Thevenin equivalent in purely local measurements based approaches.

it is practical to freeze the estimation for that time k. This has been tackled by (22) where Sig $P(u) = (u^T(k)u(k))/(n)$

$$\text{If Sig } P(u(k)) < \nu \Longrightarrow y(k) = 0, \quad u(k) = [0], \quad Q_p = [0]. \tag{22}$$

Hence, ν becomes another tuning parameter and its value depends on the measured signal. The last tuning parameter is the refresh time T_r. It defines how often the dominant oscillations are to be calculated from the estimated model parameters and displayed for the operator; this is a tradeoff between the computational power of the computer on which the application is running, taking also into account how rapidly the power system varies with time.

Besides the described real-time estimation of frequency and damping, a simple algorithm has been developed to obtain the running mean value and the amplitude of oscillations. It has been solved using two self-tuning digital low-pass filters placed before and after the input bandpass filtering. The time constants of these two filters are simply taken over from the estimated dominant frequency.

C. Voltage Stability Assessment of Transmission Corridors [17]

This method further develops the ideas used for undervoltage load shedding relays. These typically detect voltage instability solely using local measurements. If voltage becomes abnormally low (below a preset threshold value), voltage instability is assumed to be present and load is disconnected with a certain time-delay until voltage returns above the threshold value. This technique is normally referred to as undervoltage load shedding (UVLS) and is still the most widely used technique to guard against voltage instability in high-voltage power networks [4]. The drawback of this method is that the voltage threshold must be set in advance, and thus the relay cannot adapt to changing operating conditions in the power system. Voltage can be fairly close to nominal even though the system is close to its maximum loadability. Therefore, voltage level alone may not be a reliable indicator of proximity to the maximum loadability.

Hence, other approaches have been developed, and the one discussed here is based on the estimation of a Thevenin equivalent of the network at a single bus have been considered. The current through a single line feeding that bus is used to estimate an equivalent Thevenin equivalent of a possibly complex network and the generation at the remote end. Numerous variations on this theme have been presented by [18] and [19]. However, a drawback of these methods is

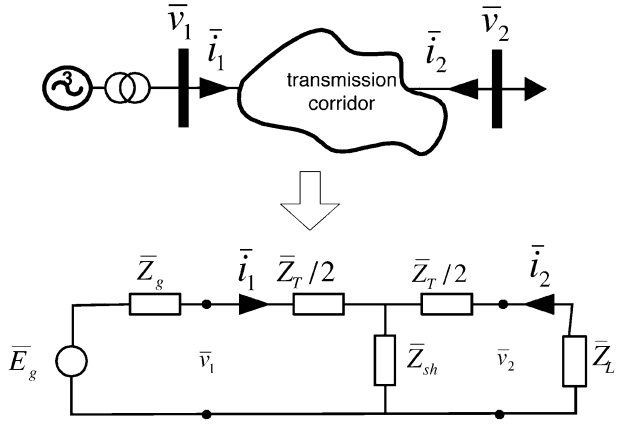

Fig. 6. T- and Thevenin representation of transmission corridor and surrounding environment.

that a single set of (local) measurements does not contain enough information to directly compute the parameters of the Thevenin equivalent. However these can, in principle, be estimated using a least-squares method once two or more sets of measurements are available (see Fig. 5). A necessary condition for accurate estimation of these parameters is that sufficient change in the measurements has occurred due to load change. During this time the feeding network and generation is assumed to remain constant. Therefore, the estimation is noise sensitive and introduces a time delay comparable to that of standard SCADA systems (several minutes). Recent developments of this approach, e.g., [20], include measurements at remote buses to assist in the estimation of the Thevenin equivalent. However, it still shows similar time delays as those observed with the local-type approaches.

The main idea of the approach proposed here is to use the measurements from both ends of the transmission corridor, thus splitting the estimation part into two stages. First, the parameters of a T-equivalent of the transmission corridor can be determined through a direct calculation and therefore without any time delay observed in local-type approaches. Second, the Thevenin equivalent of the feeding generators is computed. Once the parameters of the T- and Thevenin equivalents are known, stability analysis can be carried out analytically and various stability indicators calculated using well-known and straightforward methods [21]. The main advantage over the present state of the art is that parameters of the equivalent network can be computed from a single set of phasor measurement, and thus does not have the time delay of the local-type approaches. The calculation of the Thevenin equivalent is carried out in two stages in order to benefit from the fact that measurements at both ends of the transmission

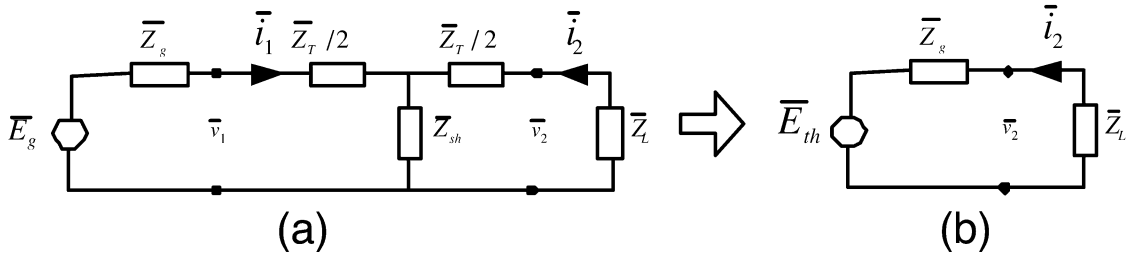

Fig. 7. Lumping of T- and Thevenin equivalents of transmission corridor and surrounding environment.

corridor are available. First, we calculate the parameters of a T-equivalent of the actual transmission corridor, including any load or generation that may be present in the transmission corridor as shown in Fig. 6.

For the measured phasors $\bar{v}_1, \bar{i}_1$ and $\bar{v}_2, \bar{i}_2$, the impedances $\bar{Z}_T, \bar{Z}_{\rm sh}$, and $\bar{Z}_L$ are given by

$$\bar{Z}_T = 2\frac{\bar{v}_1 - \bar{v}_2}{\bar{i}_1 - \bar{i}_2} \tag{23}$$

$$\bar{Z}_{\rm sh} = \frac{\bar{v}_1\bar{i}_2 - \bar{v}_2\bar{i}_1}{\bar{i}_2^2 - \bar{i}_1^2} \tag{24}$$

$$\bar{Z}_L = \frac{\bar{v}_2}{-\bar{i}_2}. \tag{25}$$

The complex voltage $\bar{E}_g$ and impedance of the equivalent voltage source $\bar{Z}_g$ cannot be simultaneously calculated in the same straightforward way, so one of them must be assumed to be known to avoid the time delay of an estimation procedure. If the generators have voltage controllers and can be assumed to stay within their capability limits, $\bar{E}_g$ can assumed to be constant and $\bar{Z}_g$ could then be calculated using

$$\bar{Z}_g = \frac{\bar{E}_g - \bar{v}_1}{\bar{i}_1}. \tag{26}$$

However, in most practical cases, it is more realistic to assume that $\bar{Z}_g$ is known, since it typically comprises the step-up transformers and short transmission line to the beginning of the transmission corridor. It is therefore preferential to calculate the equivalent complex voltage of the generators as follows:

$$\bar{E}_g = \bar{v}_1 + \bar{Z}_g\bar{i}_1 \tag{27}$$

Once we have calculated the parameters of the T- and Thevenin equivalents, a second Thevenin equivalent for the combined generation and transmission corridor can be calculated as follows:

$$\bar{Z}_{\rm th} = \frac{\bar{Z}_T}{2} + \frac{1}{\frac{1}{\bar{Z}_{\rm sh}} + \frac{1}{\bar{Z}_T/2 + \bar{Z}_g}} \tag{28}$$

and

$$\bar{E}_{\rm th} = \bar{v}_2\frac{\bar{Z}_{\rm th} + \bar{Z}_L}{\bar{Z}_L}. \tag{29}$$

Based on the second Thevenin equivalent in Fig. 7(b), stability analysis can be performed analytically. The complex power delivered to the load impedance $\bar{Z}_L$ can be written

$$\bar{S}_L = \bar{Z}_L\left|\frac{\bar{E}_{\rm th}}{\bar{Z}_{\rm th} + \bar{Z}_L}\right|^2. \tag{30}$$

Assuming that load power will evolve with constant power factor, we can set $\bar{Z}_L = k\bar{Z}_{L0}$, where k is a scale factor modeling change in the load impedance and $\bar{Z}_{L0}$ the present value of load impedance as calculated according to (25).

To find the point of maximum possible power transfer, we need to compute the maximum of

$$p_L = \Re[\bar{S}_L] = \Re\left[k\bar{Z}_{L0}\left|\frac{\bar{E}_{\rm th}}{\bar{Z}_{\rm th} + k\bar{Z}_{L0}}\right|^2\right] \tag{31}$$

with respect to the load impedance scale factor k. Differentiating (31) and solving for the first- and second-order conditions, we find that the critical load scale factor, where no further increase in p_L is possible, is given by

$$k_{\rm crit} = \left|\frac{\bar{Z}_{\rm th}}{\bar{Z}_{L0}}\right| \tag{32}$$

yielding the maximum deliverable power as

$$p_{L\,\max} = \Re\left[\bar{Z}_{\rm th}\left|\frac{\bar{E}_{\rm th}}{2\bar{Z}_{\rm th}}\right|^2\right] \tag{33}$$

Extensive field measurements reported by [22] have shown that normally at least part of the load has constant power characteristics, and the point of maximum power transfer as given by (33) then also becomes a loadability limit. Past this limit, there is a loss of equilibrium and voltage collapse will occur [21]. Equation (33) therefore also becomes a stability limit.

The voltage $\bar{v}_2$ at the virtual load bus is given by

$$\bar{v}_2 = \bar{E}_{\rm th}\frac{k\bar{Z}_{L0}}{\bar{Z}_{\rm th} + k\bar{Z}_{L0}}. \tag{34}$$

Based on (32)–(34), various stability margins can be defined as follows; In terms of load impedance (in percentages)

$$\text{MARGIN}_Z = 100(1 - k_{\rm crit}) \tag{35}$$

in terms of active power delivered to the load bus [per unit (p.u.)]

$$\text{MARGIN}_P = \begin{cases} p_{L\max} - p_L & \text{if } \bar{Z}_L > \bar{Z}_{\text{th}} \\ 0 & \text{if } \bar{Z}_L < \bar{Z}_{\text{th}} \end{cases}. \quad (36)$$

For example, if the value calculated by (36) is 4 p.u., voltage instability will occur if the active power load increase is larger than 4 p.u.

D. Voltage Stability Assessment of Meshed Networks [23]

The method described in this section is applicable to meshed network topologies. On the other hand, they require more detailed input data and more measurement points to be applicable for online use. We assume that a wide-area measurement system is available to provide a complete snapshot of the complete system state and topology with regular intervals. Using the snapshot data, a load increase is simulated on a number of selected buses until the point of maximum loadability is reached. In mathematical terms, the general formulation is

$$\begin{aligned} \text{maximize} \quad & f(p,x) \\ \text{subject to} \quad & g(p,x) = 0 \\ & h(p,x) \leq 0. \end{aligned} \quad (37)$$

The function to maximize $f(p,x)$ can be arbitrarily chosen based on the criteria to be optimized, but is in this case chosen as a fictitious active power transfer to a set of load buses known *a priori* to be critical for the voltage stability or the transfer to a predefined critical area or through a corridor. The optimization variable p can be scalar or vector valued and is the parameter that is varied to simulate a load increase. The function $g(p,x)$ represents the constraints given by the network equations as well as the steady state response of the FACTS control systems and other controllers. The function $h(p,x)$ contains various operational constraints such as voltage or current limits and actuator limits of the FACTS devices. The vector x contains the (static) state variables of the network equations and are implicitly determined by the equality constraints.

Although these methods have originally been intended for offline studies, they are applicable also for online application if the system to be studied is modeled with a moderate level of detail, which is usually the case in a wide-area measurement system. Often it is enough to model the highest one or two voltage levels. For online applications, a response time of tens of seconds is acceptable, since we here consider only the static aspects of voltage stability. A power margin with respect to voltage stability can be estimated if the optimization criteria $f(p,x)$ are customized to reflect the transfer to region for which the power margin is to be computed. From the solution of (37), the maximum allowable transfer to the region can be computed and a power margin taken as the difference between the maximum transfer and the transfer at the current operating point. Before the solution, an admittance matrix is constructed based on the snapshot from the wide-area measurement system. This admittance matrix is required to evaluate the function $g(p,x,u)$. If desired, N-1 contingency screening can be done by repeated solution of the optimization problem. By a slight modification of (37), we can extend the method so that it also generates the optimal setpoints for FACTS devices and generator voltage regulators such that the loadability of the system is maximized. The solution of (37) yields the optimal FACTS setpoints as well as the maximum loadability provided these setpoints are applied. FACTS setpoints that maximize the loadability can also be precomputed for a list of credible disturbance if contingency screening is applied using the method.

E. Line Temperature Monitoring

If the maximal power flow in a line is not constrained by any stability concern, then the heating of the line by flowing current sets the limit. This limit is predefined for very inconvenient conditions—high ambient temperature and no wind, i.e., no cooling factors. But this may be a very rare situation, so most of the time the line transfer limit may be higher in reality [24]. We propose the online method for the monitoring of the line temperature. The principle is very simple and is based on measuring the voltage and current phasors at both ends of the supervised line. Using these measurements, the variation of the line resistance can be observed. When the material properties of the line are known (i.e., the thermal dependence of the material resistance), the average temperature of the conductor can be determined.

IV. Availability of WAMC System

In this section, we focus on the availability of the hardware part of the WAMC system. The overall system availability is determined using the relations between the subsystems:

- measurement devices—PMUs;
- communication system—very individual, varying from installation to installation;
- central computation unit—PC.

The particular algorithm to be implemented in a WAMC system plays a significant role in the availability requirements of the subsystems and their mutual relations. This can be explained using the following examples (no redundancy in form of parallel use of the equipment is assumed).

- Voltage instability assessment of the transmission corridors—As described in the previous section, the current and voltage phasors are measured at both ends of the transmission corridor. When any of these measurements is missing, the algorithm cannot provide the result. Therefore, all subsystems must be considered for the availability assessment to be fully operable.
- Voltage instability assessment of meshed networks—Full network observability is necessary for this algorithm. However, the outage of one PMU can be compensated for in the state estimation procedure, which alleviates the availability requirement on the data acquisition subsystem, i.e., the PMUs.
- Oscillations assessment—The filtering technique described in the previous section can extract the oscillations parameters (frequency, damping, etc.) from basically any signal provided by a PMU. Of course,

the observation of the local modes at the locations, from which no data is available, is not possible. However, this does not influence the detection process for all the other locations. Thus, we assume that the loss of communication to one substation (where several PMUs can be located) can be tolerated.

The overall WAMC system availability can be increased using the traditional method of reinforcing and backing up the subsystems from which it is composed.

- Central computation unit—An additional computer working in parallel with the existing one can be installed.
- Communication system—The connection between the substation and the central location can be reinforced either by adding a parallel link or meshing the WAN by interconnecting also the substations with each other.
- Measurement devices—Appropriate redundancy constraints can be introduced in the optimal PMU placement procedure [25].

V. Cost Worth Assessment

Reference [26] analyzed the investment in the WAMC systems as an alternative to the building of traditional transmission systems assets, i.e., line connecting two areas with the trade limited by the congestion. Here the focus is on WAMC as the alternative to traditional protection schemes. Therefore, the assessment criteria can be linked to the power system performance from the reliability and availability point of view. The reliability of the power system is usually expressed in terms of the reliability indexes. Many of them have been proposed; e.g., expected energy not supplied (EENS) may be adopted. The evaluation procedure similar to [27] can be applied. However, we propose a use of the ac power flow based computations, since we want to consider the voltage stability problems as well. The link to monetary aspects of WAMC systems can then be established via EENS. One possibility is to estimate the overall society impact with respect to the amount of undelivered energy and durations of the interruptions. Another possibility is to look at the performance over investment factor of a WAMC system: $-\triangle \text{EENS}/\triangle \text{price}$, where the goal would be to maximize it, i.e., to increase the reliability of the network while spending as little as possible for it. Both evaluation factors can be used to compare WAMC systems with other alternative solutions for a particular power system, e.g., the WAMC system and undervoltage load shedding system based on the local relays.

VI. Example

We use the part of the realistic power system shown in Fig. 8 to demonstrate the above-described algorithms and methodologies in a consistent manner/form. The northern (upper) part of the power system represents the area with the dominant generation whereas the southern (bottom) part the area with the dominant consumption. Therefore, the lines connecting these areas are subjected to a heavy power flow. This results in the high sensitivity of the system to outages. The occurring problems include almost all types of instabilities, often having severe consequences in the form of partial or even systemwide blackouts. The installation of WAMC could significantly reduce this risk. Therefore, we study in this section how the most important practical aspects are considered. The steps leading to the installation of WAMC are:

1) identification of the causes of the network vulnerabilities;
2) selection and simulation of the WAMC algorithms;
3) design of the system setup;
4) availability assessment of the WAMC system;
5) cost worth assessment study.

The records of the severe network disturbances and the dynamic simulations of the selected scenarios are used to discover the system properties and tendency to the instabilities. The voltage instability and the power oscillations are the worst threats for this network. Therefore, we demonstrate the algorithms assessing these phenomena.

A. Application of Voltage Stability Assessment for Transmission Corridors

When a WAMC system installation with complete observability is not available and the network considered has clearly defined corridors, the approximate voltage instability assessment is suitable. In the case study considered here, 17 phasors must be measured to provide this algorithm with the necessary data as compared with the 54 required for complete observability.

Consider the network diagram in Fig. 8. This network has a longitudinal structure with a clearly defined generation area in the northern end above Cut 1. Generation here is about 2440 MW and the local load is about 578 MW and contains also shunt reactors rated at a total of 275 MVAr. The southern end is a load area with about 2159 MW of load and 700-MW local generation. Between the cuts is a transmission corridor with five parallel transmission lines but also about 300 MW of load. References to per unit quantities are made on a 100-MVA basis. All machines are equipped with voltage controllers and reactive power limiters, and the generators in the northern part of the system are also using governor control. The generators in the southern part are using constant power governor models and have reactive power limiters. Loads are modeled using exponential recovery dynamic load models. To apply the transmission corridor voltage instability assessment to this network, we must model the five parallel lines as a single-corridor equivalent. We define the corridor boundaries as the buses neighboring the two cuts on either side of the corridor. After identifying these boundaries, which are given by the two transfer cuts, we can define two virtual buses, one for each end of the transmission corridor. These are the buses directly adjacent to a cut. Buses 6, 13, and 14 of the original system are grouped into virtual bus 1, and buses 24, 15, and 16 into virtual bus 2. The part of the system between cuts 1 and 2 becomes the virtual transmission corridor. At least one voltage in the area of each virtual bus and the currents on each line crossing the cut must be

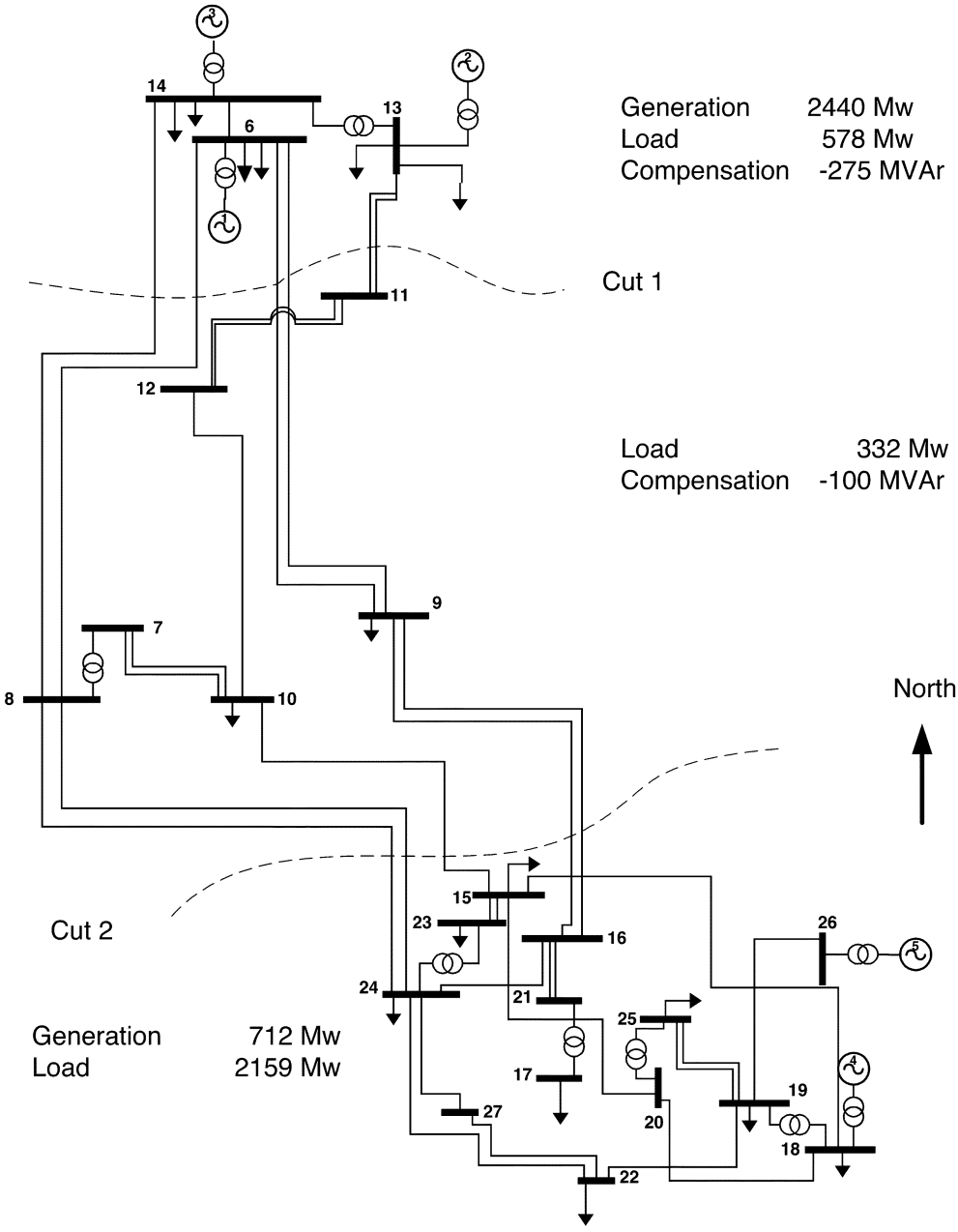

Fig. 8. Example network diagram, showing a part of an actual network with the transmission corridor enclosed by transfer cuts.

measured. We can then compute the currents at either end of the virtual transmission corridor using

$$\bar{i}_i = \left(\frac{p_{\text{cut}-i} + jq_{\text{cut}-i}}{\bar{v}_i} \right)^* \quad i \in 1, 2. \tag{38}$$

For example, here $p_{\text{cut}-i}$ and $q_{\text{cut}-i}$ refer to the sum of the power transfers through cut i and $\bar{v}_i$ as the average of the voltages of the buses included in in virtual bus i.

Fig. 9 shows the simulation results where the the two lines between buses 9 and 16 are tripped at 20 and 30 s, which is a disturbance that makes the system unstable, and it eventually collapses at about 82 s. The top-left figure shows the calculated voltages of the two virtual buses, and the top right figure shows the so-called PV-curve, where the maximum power transfer given by (33) is clearly illustrated. The rightmost point of this curve corresponds to the stability boundary where $k = k_{\text{crit}}$ (or, equivalently, $\bar{Z}_t h = \bar{Z}_L$). In this case, the stability boundary is crossed at about 60 s, and the collapse of the system progresses rapidly after this point. The two lowermost plot shows the estimated Thevenin impedance, load impedance, and voltage. In the bottom left plot, the stability boundary is given by the intersection of the curves for the Thevenin and load impedances. For stability control, load shedding can be based on the proximity to the point of maximum loading according to (35)–(36) or a sudden drop of the estimated Thevenin voltage $\bar{E}_{\text{th}}$.

B. Voltage Stability Assessment of Meshed Networks

In networks where transmission corridors cannot be as easily identified, or where generation and load are more

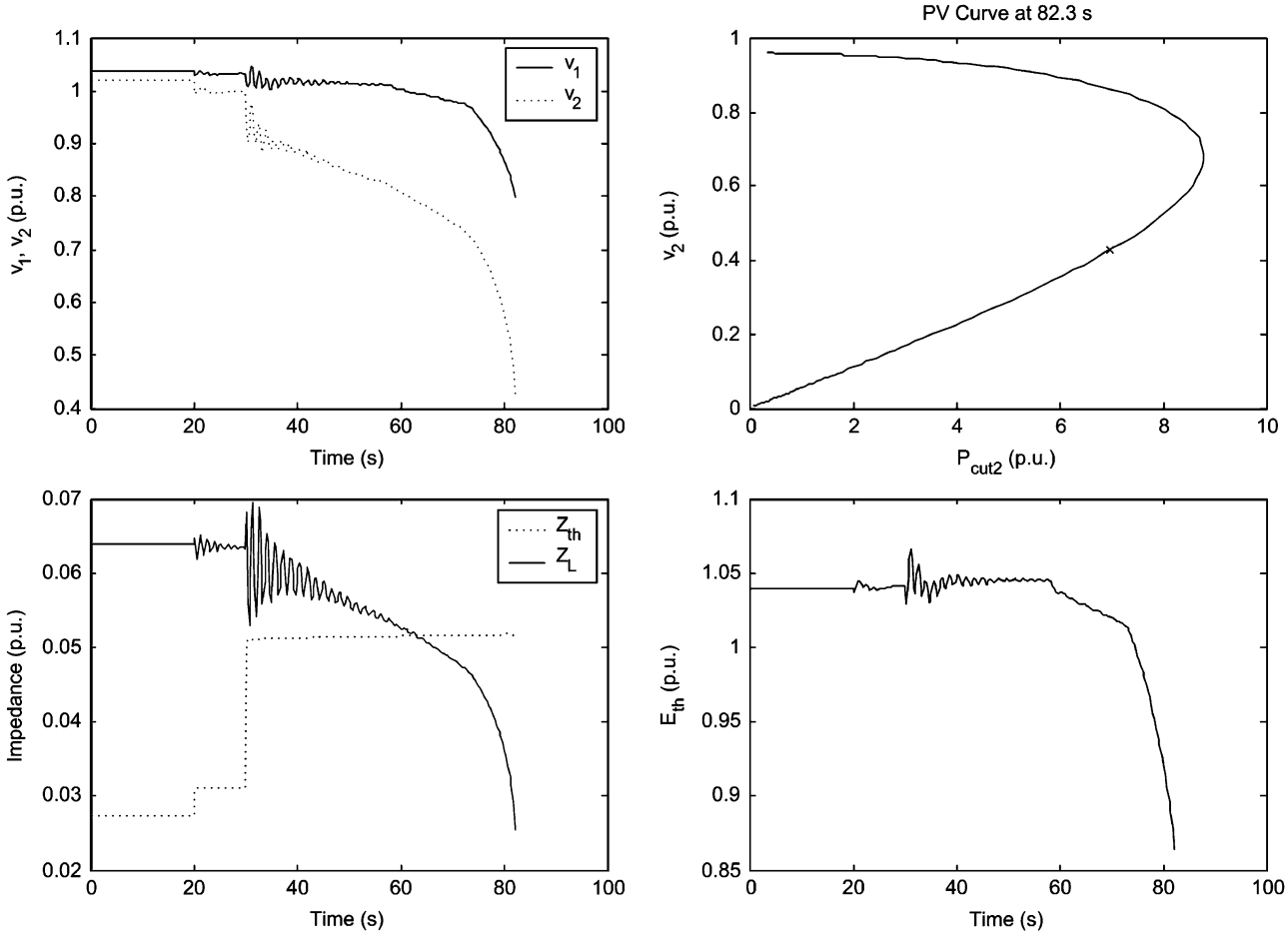

Fig. 9. Simulation results for tripping of the two lines between buses 9 and 16 at 20 and 30 s, respectively.

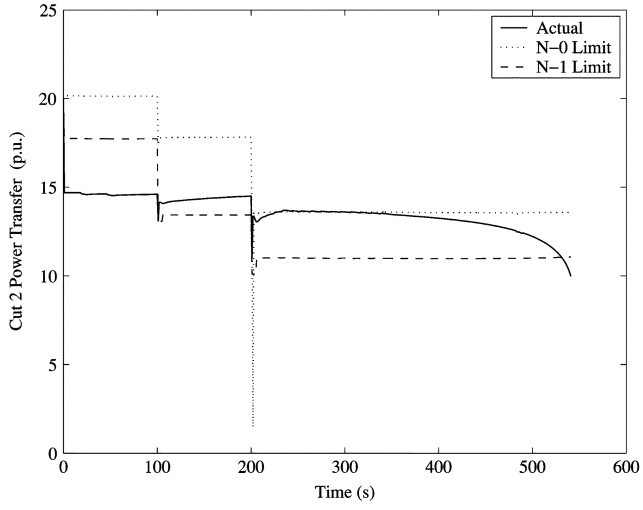

Fig. 10. Result of $\mathrm{N}-0$ and $\mathrm{N}-1$ loadability computation during double line trip scenario.

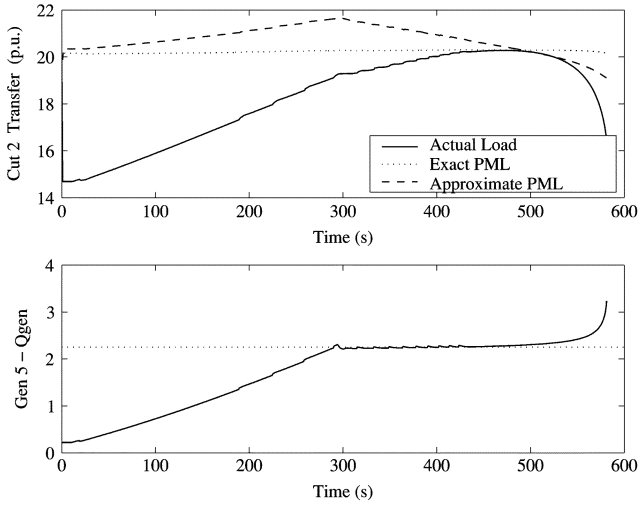

Fig. 11. Result of approximate voltage stability assessment and exact loadability calculation computation during load ramp scenario. The bottom part of the figure shows the reactive power produced by generator 5.

evenly distributed, the simple method in the previous section cannot be applied. With the assessment based on complete observability, a snapshot from the state estimation application is used as input data for the optimization. For the test case here, 54 phasors must be measured to carry out the topology and state estimation. We define the objective function for the loadability calculation as the sum of the active power transfer through Cut 2. Fig. 10 shows the $N-1$ and $N-0$ stability limits as the actual power transfer through Cut 2 during the line trip scenario. The $N-0$ limit is computed once a second and the $N-1$ margin every 5 s.

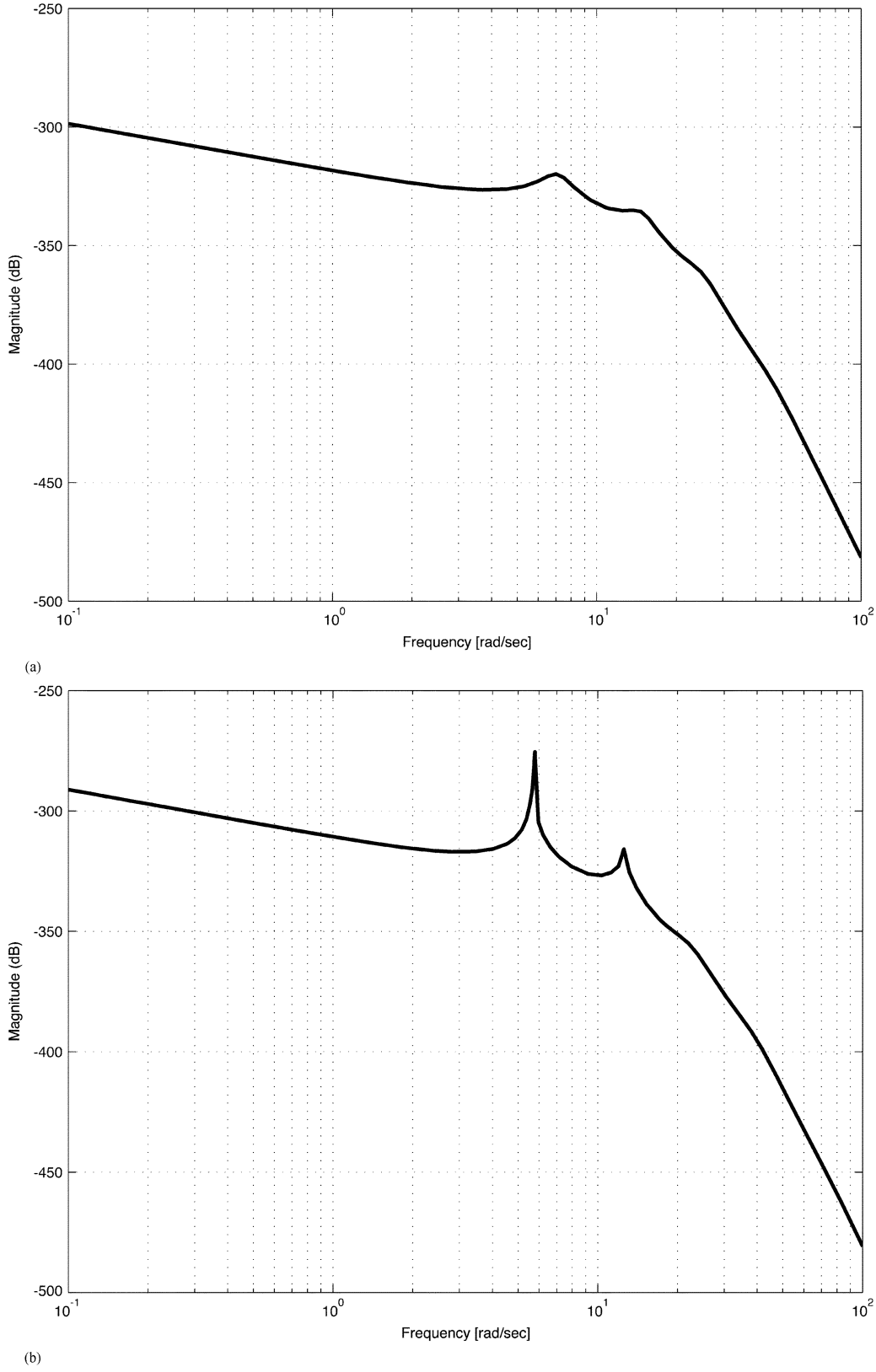

Fig. 12. Spectra of the estimated AR model for two different parameter sets $a_i(k)$ frozen for $k = 750$ s (top) and $k = 810$ s (bottom); see also Fig. 13.

Following the first trip, the margin to the $N - 0$ limit is about 4 p.u. and directly after the second trip around 0.5 p.u. As the load dynamics restore the load to its predisturbance value, the actual load crosses the $N - 0$ stability limit and after that the collapse is rapid. Note that the actual load is actually higher than the $N - 0$ limit for a short period of time. This is due to the overexcitation limiters of the generators models allowing an overload for a short period of time. This effect is not modeled in the steady-state model used for the loadability computation. From this comparison,

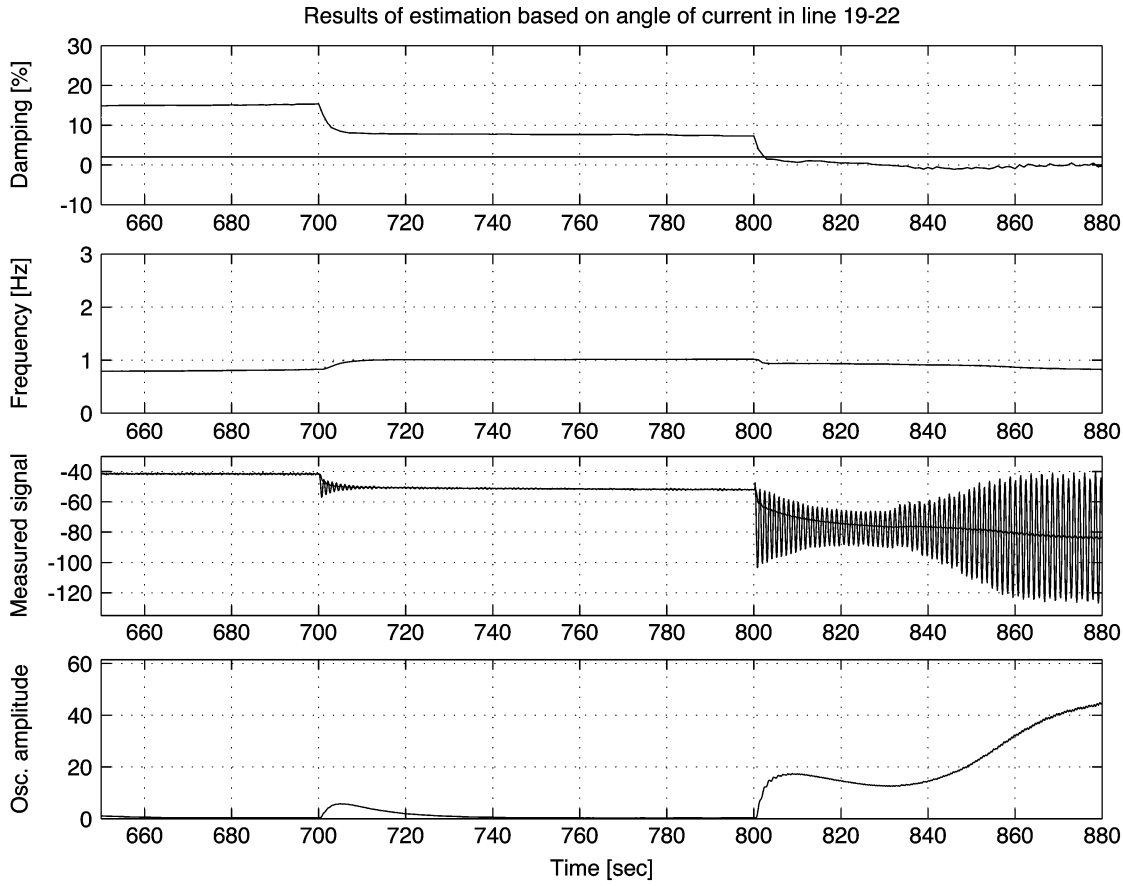

Fig. 13. Results of the detection of oscillations in time domain: plots show (from the top to the bottom) estimated dominant relative damping and frequency, the measured signal and the amplitude of the oscillation.

we can see that the $N - 0$ limit can be used to accurately compute the current distance from the maximum loadability. The $N - 1$ margin is about -1 p.u following the first line trip. That is, from the $N - 1$ margin we can predict that the system would be at or beyond its maximum loadability capability if the worst contingency should occur.

It is also interesting to compare the result of the exact optimization based assessment with the approximate version used for the corridor case. Fig. 11 shows the results of the approximate voltage stability assessment for the load ramp scenario. The top figure shows the variation of the predicted maximum transfer capability as the load in the southern area is increased as well as the "exact" limit provided by the optimization method. Initially, the predicted maximum capacity is close to the true maximum loadability 20.4 p.u. As the load increase progresses, the generators in the southern region will supply more reactive power such that the voltage is kept close to nominal. The method is based on an assumption that the load will evolve with constant factor from any given point in time and will thus assume that the support from the generators will continue even with high loading. During the time until 300 s, the predicted maximum loadability increases as the generators provide more and more reactive support. Since the approximate method assumes that there is only a voltage source at the northern end, its internal model is not very accurate at this time. Therefore, an approximate method gives an overly optimistic estimate of the transfer capacity and overestimates the capacity by a maximum 10% at time 300 s. Once the reactive power limiters are activated, the internal model used by the approximate method becomes more accurate and the error decreases as the operating point moves closer to the point of the maximum loadability. Close to this point, there is only a marginal estimation error. In general, the method will always be accurate around the maximum loadability, but a certain error in the predicted power margin can be expected when operating far from it.

C. Oscillation Stability Assessment

A model of a real power system is shown in Fig. 8. The reduced model consists of 157 physical states and 112 output channels where PMUs are installed. Measured signals are sampled at 10 Hz. Based on the results of modal analysis, a suitable signal was selected to detect the dominant inter-area oscillation between the generator groups G1, G2, and G3 (north) and G4 and G5 (south). To make the simulation more complicated and realistic, white noise having a signal-to-noise ratio of 40 db was added (measurement error 1%; signal $d(k)$ to the measured signal before feeding it into the estimation procedure. Typical results in detection of oscillations in frequency and time domain are shown in Figs. 12 and 13. The following situation has been studied on the power system:

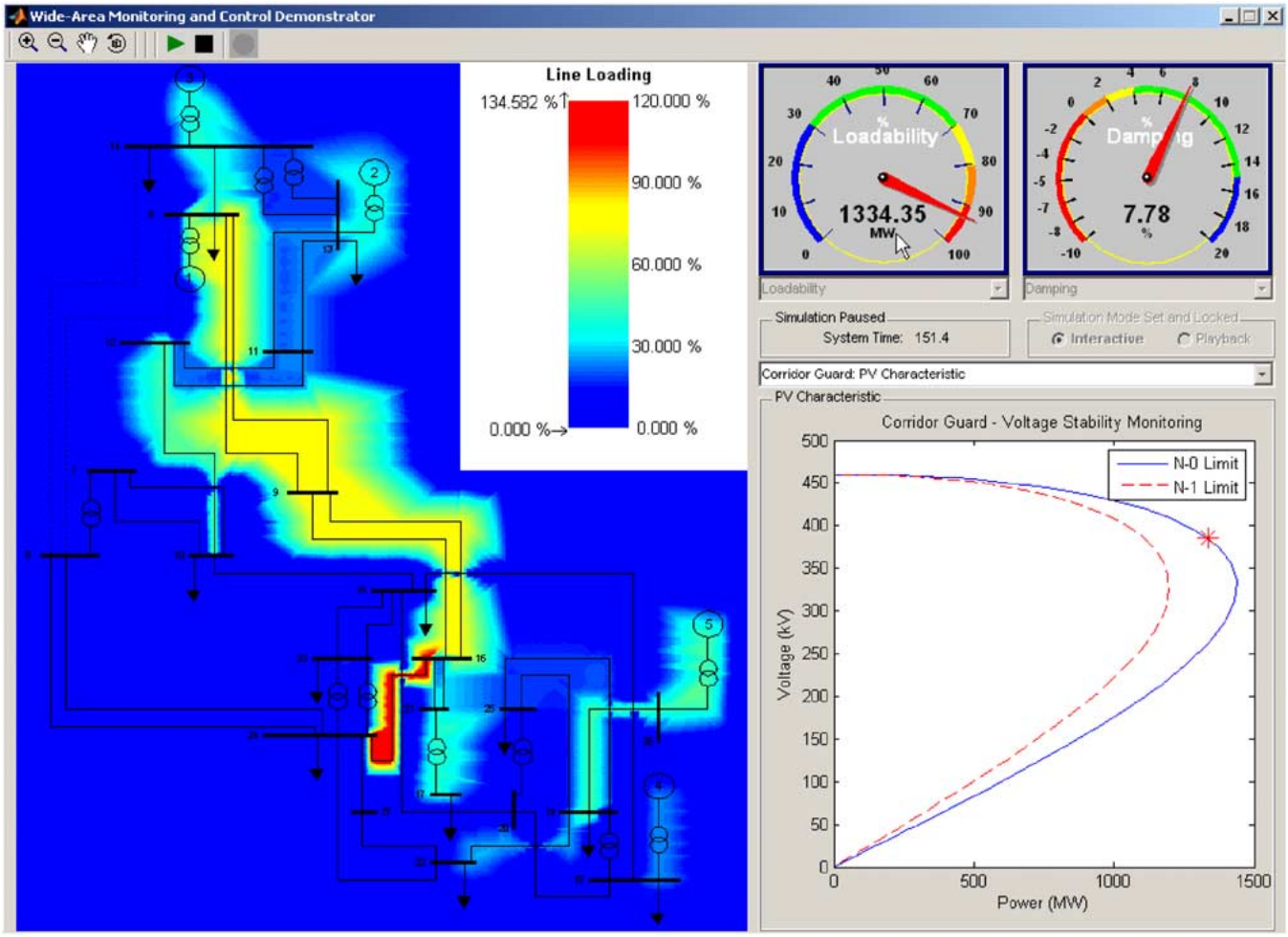

Fig. 14. GUI example.

- · · ·–700 s: normal operation of the power system;
- 700–800 s: disconnecting one line between nodes 9 and 16;
- 800–· · · s: disconnecting second line between 9 and 16.

D. GUI

The results of the various applications and in some cases the raw data are visualized by a GUI. An example display is shown in Fig. 14. Two gauges are set to display important parameters such as transmission corridor loadability (in the left gauge, top right) and damping of power oscillations on the transmission corridor (in the right gauge, top right). Line loading is demonstrated using a contour map, where overloads are represented in red for easy identification. Finally, the loadability of the transmission corridor, obtained from the voltage stability assessment, is represented on the PV curve in the lower right corner. Other possibilities include contour mapping, two-dimensional and three-dimensional dynamics visualizations, line power oscillation visualizations, voltage stability indicator, contingency assessment, oscillatory stability indicator, islanding identification, and gauges [28].

E. Availability Assessment

In the availability assessment, we provide the numerical results for the three applications with no redundancy as already discussed. We assume that all PMUs are from the same vendor as well as the communication links (here we consider the most common communication connection composed of the Star coupler, Gateway, two modems, and a phone line, all connected in series; see Fig. 2).

- Voltage instability assessment of the transmission corridors—All components of the WAMC setup must be in the operational state; therefore, the overall availability is obtained

$$A = A_{\text{pc}} \cdot A_{\text{com1}} \cdot A_{\text{pmu1}} \tag{39}$$

where

$$A_{\text{com1}} = \prod_{j=1}^{\text{no. of substation}} A_j \tag{40}$$

$$A_{\text{pmu1}} = \prod_{i=1}^{\text{no. of PMUs}} A_i. \tag{41}$$

Note that the reduced WAMC setup supervising only the corridor is used. This represents six PMUs, six communication channels, and one PC. Inserting the typical component availability values, the overall WAMC system availability is 0.99793338285509.

- Voltage instability assessment of meshed networks—In this case, the overall availability as well as the availability of the communication system is computed using the same equation as in the previous bullet. The availability of PMUs is computed as follows:

$$A_{\mathrm{pmu2}} = \prod_{i=1}^{\text{no. of PMUs}} A_i + \sum_{j=1}^{\text{no. of PMUs}} \left[\frac{(1-A_j)}{A_j} \prod_{i=1}^{\text{no. of PMUs}} A_i \right] \quad (42)$$

where the first term refers to the probability that all PMUs are available and the second term to the probability that one PMU is out of service whereas the others are available. The full network observability setup includes 11 PMUs placed in six substations $=>$ six communication channels and one PC. Solving (42), the availability 0.99807706227163 has been achieved.

- Oscillations assessment—If the setup for the full network observability is used also for this algorithm, the availabilities of the communication system and PMUs should not be calculated separately as in the previous cases. The reason is that we accept the outage of the communication link to one substation

$$A_{\mathrm{com,pmu}} = A_{\mathrm{com1}} \cdot A_{\mathrm{pmu2}} + \sum_{k=1}^{\text{no. of substations}} \times \left[\frac{(1-A_k)}{A_k} \prod_{j=1}^{\text{no. of substations}} A_j \right] \cdot \left[\prod_{i=1}^{\text{no. of PMUs in connected substations}} \right]. \quad (43)$$

The first term expresses the probability that all communication links are available and one PMU is not, and the second term expresses the probability that one communication link is unavailable and all PMUs in remaining substations are available. The overall WAMC hardware availability is then 0.99999800393207.

VII. Conclusion

The aim of this paper was to show the feasibility of WAMC systems. First, it was shown how the conventional SCADA/EMS systems could be extended/complemented to incorporate dynamic measurement data from PMUs. Possible software architecture for such a system was outlined. Then a number of power system applications concerning monitoring and emergence control were discussed: frequency instability assessment, oscillation detection assessment, voltage stability assessment, and line temperature monitoring. The proposed scheme is demonstrated in a real power system, and its virtues are shown. A cost worth assessment is made. The discussion and the findings of the paper show that technologies and software exist that can be used to design and implement WAMC systems. It is further shown that such a system can be used to enhance the security of power systems by providing real-time monitoring of key quantities and by enabling emergency control. The future work shall focus on the aspects related to the closing the control loop in practical WAMC systems, in particular the performance issues of the platform.

References

[1] A. Phadke, J. S. Thorp, and K. J. Karimi, "State estimation with phasor measurments," *IEEE Trans. Power Syst.*, vol. 1, no. 1, pp. 233–241, Feb. 1986.

[2] C. Rehtanz, M. Larsson, M. Zima, M. Kaba, and J. Bertsch, "System for wide area protection, control, and optimization based on phasor measurements,," presented at the Conf. Power Systems and Communication Systems Infrastructures for the Future, Beijing, China, 2002.

[3] M. Larsson and C. Rehtanz, "Predictive frequency stability control based on wide-area phasor measurements," in *IEEE Power Engineering Soc. Summer Meeting*, vol. 1, 2002, pp. 233–238.

[4] CIGRE Task Force 38.02.19, "System protection schemes in power networks,", Paris, France, Ref. No. 187, 2000.

[5] P. M. Anderson and M. Mirheydar, "A low-order system frequency response model," *IEEE Trans. Power Syst.*, vol. 5, no. 4, pp. 720–729, Aug. 1990.

[6] ——, "An adaptive method far setting underfrequency load shedding relays," *IEEE Trans. Power Syst.*, vol. 7, no. 2, pp. 647–655, May 1992.

[7] D. Novosel, K. T. Vu, D. Hart, and E. Udren, "Practical protection and control strategies during large power-system disturbances,," in *Proc. 1996 IEEE Transmission and Distribution Conf.*, pp. 560–565.

[8] S. J. Huang and C. C. Huang, "An adaptive load shedding method with time-based design for isolated power systems,," *Elec. Power Energy Syst*, vol. 22, pp. 51–58, 2000.

[9] V. N. Chuvychin, N. S. Gurov, S. S. Venkata, and R. E. Brown, "An adaptive approach to load shedding and spinning reserve control during underfrequency conditions,," *IEEE Trans. Power Syst.*, vol. 11, no. 4, pp. 1805–1810, Nov. 1996.

[10] O. Rogers, *Power System Oscillations*. Norwell, MA: Kluwer, 2000.

[11] P. Korba, M. Larsson, and C. Rehtanz, "Detection of oscillations in electric power systems using kalman filtering techniques," in *Proc. IEEE Conf. Control Applications*, vol. 1, 2003, pp. 183–188.

[12] M. Hemmingsson, O. Samuelsson, K. Pedersen, and A. Nielsen, "Estimation electro-mechanical parameters using frequency measurements," presented at the IEEE Power Engineering Soc. Winter Meeting, Columbus, OH, 2001.

[13] J. Hauer, "Application of prony analysis to the determination of modal content and equivalent models for measured power system response," *IEEE Trans. Power Syst.*, vol. 6, no. 3, pp. 1062–1068, Aug. 1991.

[14] O. Ledwich and E. Palmer, "Modal estimates from normal operation of power systems," presented at the IEEE Power Engineering Soc. Summer Meeting, Singapore, 2000.

[15] S. Haykin, *Adaptive Filter Theory*. Englewood Cliffs, NJ: Prentice-Hall, 1996.

[16] J. Proakis and D. Monolakis, *Introduction to Signal Processing*. New York: Macmillan, 1987.

[17] M. Larsson, C. Rehtanz, and J. Bertsch, "Real-time voltage stability assessment of transmission corridors," presented at the IFAC Symp. Power Plants and Power Systems Control, Seoul, Korea, 2002.

[18] R. Balanathan, N. C. Pahalawaththa, U. D. Annakkage, and P. W. Sharp, "Undervoltage load shedding to avoid voltage instability,," *IEE Proc. Generat., Transmis., Distribut.*, vol. 145, no. 2, pp. 175–181, Mar. 1998.

[19] W. H. Quantaince *et al.*, "Method and device for assessing the stability of an electric power transmission network," U.S. Patent Appl. No. 20 020 123 849, 20 020 097 055, 20 010 021 896, 2001.
[20] L. Warland and A. T. Holen, "Estimation of distance to voltage collapse: Testing an algorithm based on local measurements,," presented at the Power Systems Computation Conf., Sevilla, Spain, 2002.
[21] T. V. Cutsem and C. Vournas, *Voltage Stability of Electric Power Systems*, ser. Power Electronics and Power Systems Series. Norwell, MA: Kluwer Academic Publishers, 1998.
[22] D. Karlsson and D. J. Hill, "Modeling and identification of nonlinear dynamic loads in power systems," *IEEE Trans. Power Syst.*, vol. 9, no. 1, pp. 157–163, Feb. 1994.
[23] M. Larsson, C. Rehtanz, and D. Westermann, "Improvement of cross-border trading capabilities through OPF-based control of FACTS," Automat. Electr. Power Syst., 2004. submitted, submitted for publication.
[24] S. D. Foss, S. H. Lin, and R. A. Fernandez, "Dynamic thermal line ratings—Part 1—Dynamic ampacity rating algorithm," *IEEE Trans. Power App. Syst.*, vol. PAS-102, no. 6, pp. 1858–1864, Jun. 1983.
[25] P. Jansson, "Optimal placement of phasor measurement units in power systems with redundancy and detection of topology as constraints," M.S. Thesis, Uppsala Univ., Uppsala, Sweden, 2002.
[26] C. Rehtanz and D. Westermann, "Wide area measurement and control system for increasing transmission capacity in deregulated energy markets," presented at the Power Systems Computation Conf., Sevilla, Spain, 2002.
[27] A. M. L. da Silva *et al.*, "Transmission capacity: Availability, maximum transfer, and reliability," *IEEE Trans. Power Syst.*, vol. 17, no. 3, pp. 843–849, Aug. 2002.
[28] M. Larsson, R. Gardner, and C. Rehtanz, "Interactive simulation and visualization of wide-area monitoring and control applications," in *Proc. Power Systems Computation Conf.*, Liège, Belgium, 2005, submitted for publication.

Marek Zima (Student Member, IEEE) received the B.Sc. degree in electric power engineering from Slovak University of Technology, Bratislava, Slovakia, in 1999 and the M.Sc. degree in electric power engineering from the Royal Institute of Technology (KTH), Stockholm, Sweden in 2001. He is currently working toward the Ph.D. degree in the Power Systems Laboratory, Swiss Federal Institute of Technology (ETH), Zürich

Since 2001, he has been with ABB Switzerland, Zürich, where he is involved in the research and development of the wide-area platform for monitoring and control. His research interests are stability issues and analysis and control of power systems.

Mats Larsson (Member, IEEE) received the M.S. degree in computer science and engineering, the Licentiate degree in industrial automation, and the Ph.D. degree in industrial automation from Lund University, Lund, Sweden in 1993, 1997, and 2001, respectively.

Since 2001, he has been with Corporate Research, ABB Switzerland, Baden-Dättwil, working on the research and development of wide-area stability controls for power systems. His research interests are power system stability, optimal control, and artificial intelligence applications in power systems.

Petr Korba received the M.Sc. degree in electrical engineering from the Czech Technical University, Prague, in 1995 and the Ph.D. degree (with honors) from the University of Duisburg, Duisburg, Germany, in 2000.

He was an Invited Scientist at the Delft University of Technology, Delft, the Netherlands, and at the University of Manchester Institute of Science and Technology (UMIST) Manchester, U.K., in 1998 and 1999, respectively. He became a member of staff at UMIST, Control Systems Centre, where he stayed until 2001. He then joined ABB Switzerland Ltd. He is currently with Corporate Research, ABB Switzerland, Baden-Dättwil. His interests include model identification techniques, robust and adaptive control theory and their industrial applications.

Dr. Korba received the 2000 American Control Conference Best Paper Award.

Christian Rehtanz (Senior Member, IEEE) received the Diploma degree in electrical engineering and the Ph.D. degree from the University of Dortmund, Dortmund, Germany, in 1994 and 1997, respectively.

From 2000 to 2003, he was with ABB Corporate Research, Switzerland, and from 2003 to 2005 he was Head of Technology for the global ABB Power Systems business area. Since 2005, he has been Director of ABB Corporate Research, Beijing, China. He is also a Part-Time Lecturer at the Swiss Federal Institute of Technology, Zürich. His research activities include technologies for network enhancement and congestion relief like stability assessment, wide-area monitoring, protection, and coordinated Flexible AC Transmission Systems (FACTS) and HVdc control.

Göran Andersson (Fellow, IEEE) received the M.S. and Ph.D. degrees from the University of Lund, Lund, Sweden, in 1975 and 1980, respectively.

In 1980, he joined ASEA's HVdc division, and in 1986 he was appointed Professor in Electric Power Systems at the Royal Institute of Technology, Stockholm, Sweden. In 2000, he was appointed to his current position as a Professor at the Power Systems Laboratory, Swiss Federal Institute of Technology, Zürich. His research interests are in power system analysis and control.

Prof. Andersson is a Member of the Royal Swedish Academy of Engineering Sciences and the Royal Swedish Academy of Sciences.